THE JOURNAL OF BIOLOGICAL CHEMISTRY Vol. 279, No. 10, Issue of March 5, pp. 8862–8866, 2004

Printed in U.S.A.

Organization of the AAA$^+$ Adaptor Protein PspA Is an Oligomeric Ring*[S]

Received for publication, July 21, 2003, and in revised form, December 18, 2003
Published, JBC Papers in Press, December 19, 2003, DOI 10.1074/jbc.M307889200

Ben D. Hankamer‡§, Sarah L. Elderkin§¶‖, Martin Buck¶, and Jon Nield¶**

From the ‡Institute of Molecular Bioscience, University of Queensland, Brisbane, QLD 4072, Australia and the ¶Department of Biological Sciences, Imperial College London SW7 2AZ, United Kingdom

The 25.3 kDa "adaptor" protein, PspA (phage shock protein A), is found in the cytoplasm and in association with the inner membrane of certain bacteria. PspA plays critical roles in negatively regulating the phage shock response and maintaining membrane integrity, especially during the export of proteins such as virulence factors. Homologues of PspA function exist for thylakoid biogenesis. Here we report the first three-dimensional reconstruction of a PspA assembly from *Escherichia coli*, visualized by electron microscopy and single particle analysis to a resolution of 30 Å. The assembly forms a 9-fold rotationally symmetric ring with an outer diameter of 200 Å, an inner diameter of 95 Å, and a height of ~85 Å. The molecular mass of the complex was calculated to be 1023 kDa by size exclusion chromatography, suggesting that each of the nine domains is likely to be composed of four PspA subunits. The functional implications of this PspA structure are discussed in terms of its interaction with the protein export machinery of the bacterial cell and its AAA$^+$ protein partner, PspF.

Virtually all bacteria are able to export a range of proteins from the cytoplasm to the cell surface, the extracellular environment, or, in the case of pathogenic bacteria, into the host cell. Protein export fulfills a wide range of functions, including the induction of virulence through the transmission of virulence factors that can induce proteolysis, cytotoxicity, or hemolysis. At least four distinct secretion mechanisms (types I-IV) have been identified (1) with the export process being mediated by complex protein assemblies. Determining the structural basis and function of export in bacterial pathogenesis has long held important implications, including the identification of potential antibacterial drug targets.

Secretin Pores—Central to protein export in certain bacteria are the secretin pores (*e.g.* PulD in *Klebsiella pneumoniae*, YscC in *Yersinea enterocolitica*, and InvG in *Salmonella typhimurium*). These are essential for the export of virulence factors across the outer bacterial membrane. Misinsertion of the secretin pores can be harmful to the bacterium. To prevent misinsertion, orchestrated insertion mechanisms involving chaperones have evolved (*e.g.* the high-fidelity insertion of PulD in *K. pneumoniae* by the outer membrane-anchored lipoprotein, PulS). In *Escherichia coli*, products of the *psp*[1] operon have been implicated in combating the effects of misinsertion. The *psp* operon is directly induced when PulD is misinserted (2) and also when the YscC secretin of *Y. enterocolitica* is misinserted due to the absence of its chaperone protein, YscW (3). Induction of the *psp* operon also occurs when the Sec pathway, which is involved in the export of proteins from the cytoplasm to the periplasm across the inner membrane, becomes blocked and results in a loss of proton motive force (4, 5). The inner membrane protein YidC functions to insert proteins into the inner membrane, either independently or cooperatively, with the Sec translocase. Interestingly, depletion of YidC results in the rapid induction of the *psp* response through a reduction in the proton motive force, possibly due to incorrect assembly of the cytochrome oxidase and F_1F_0 ATPase (6, 7). Collectively, these data suggest that the products of the *psp* operon have at least three functions as follows: (i) to confer the ability to cope with misinserted secretins into the outer membrane; (ii) to protect against blockage of the Sec dependent pathway; and, finally, (iii) to prevent incorrect insertion of proteins into the inner membrane via YidC. All these effects may be linked by a need to maintain proton motive force.

The *psp* operon has been identified in many pathogenic bacteria, including *Y. enterocolitica, Shigella flexneri*, *Salmonella typhimurium, Vibrio cholerae*, and *K. pneumoniae*. These bacteria are responsible for causing diarrhea, bacillary dysentery, gastroenteritis, cholera, and pneumonia, respectively. In a recent DNA microarray study aimed at gaining a global understanding of gene regulation during pathogenesis in *S. typhimurium*, almost a quarter of the genes underwent a change in their level of expression (8). Of these, the phage shock *psp* operon of *Salmonella* bacteria was one of the top three most highly expressed operons during infection. This finding clearly suggests that the *psp* operon fulfills a protective role during the infection process (8). Further evidence supporting the protective role of Psp proteins has emerged. In particular, the deletion of the *pspC* gene in *Y. enterocolitica* was reported to induce severe growth defects and the attenuation of virulence on the expression of *YscC* (9).

The psp Operon, AAA$^+$ Proteins, and RNA Polymerase—In *E. coli* the *psp* operon *pspABCDE* has been used as a model system in the investigation of *psp* operon regulation and function (10). The *psp* operon is transcribed by the RNA polymerase containing the σ^{54} subunit (σ^{54}-RNA polymerase) and activated

* This work was supported by the United Kingdom government Biotechnology and Biological Sciences Research Council. The costs of publication of this article were defrayed in part by the payment of page charges. This article must therefore be hereby marked "*advertisement*" in accordance with 18 U.S.C. Section 1734 solely to indicate this fact.

[S] The on-line version of this article (available at http://www.jbc.org) contains a Euler angle map.

§ These authors have contributed equally to this work.

‖ Grateful recipient of a Biotechnology and Biological Sciences Research Council studentship. Present address: Marie Curie Research Institute, The Chart, Oxted, Surrey RH8 0TL, United Kingdom.

** Holder of a Royal Society University Research Fellowship and to whom correspondence should be addressed. E-mail: j.nield@imperial.ac.uk.

[1] The abbreviations used are: Psp, phage shock protein; CHAPS, 3-[(3-cholamidopropyl)dimethylammonio]-1-propanesulfonic acid; SEC, size exclusion chromatography; HPLC, high performance liquid chromatography; EM, electron microscopy; TBS, Tris-buffered saline.

by an additional protein, PspF, which is a member of the AAA$^+$ protein family (ATPase associated with a variety of cellular activities). PspF itself is divergently transcribed from the *pspABCDE* operon (10, 11). PspF is able to bind and hydrolyze ATP by using the derived energy to remodel the σ^{54}-RNA polymerase. The PspA protein forms a complex with PspF, thereby inhibiting its function by stopping its ATPase activity, either by preventing nucleotide access to the active site or by inhibiting formation of the correct oligomeric form (12). PspA has recently been classified as an "adaptor" protein working with PspF (12–14). Notably, a homologue of PspA, VIPP1, is involved in the thylakoid biogenesis of *Synechocystis* spp. (15) and the higher plant *Arabidopsis thaliana* (16).

Here we present the first three-dimensional structure of a macromolecular assembly of *E. coli* PspA determined by electron microscopy on negatively stained particles and discuss how it might relate to cytoplasmic adaptor and membrane-associated functions. Together, these data suggest that PspA has a role in membrane integrity and is essential for the adaptation to membrane stress imposed by the misinsertion of the components of the secretin pore.

MATERIALS AND METHODS

Preparation of the PspA Complex—Plasmids, DNA manipulations, protein purification, and related analyses by SDS-PAGE and Western blotting have been described previously (12). Modification of the PspA purification protocol included the omission of 1.1% CHAPS from fractions prior to dialysis. Instead, these fractions were dialyzed for 2 h in buffer 1 (200 mM NaCl, 75 mM NaSCN, and 20 mM Tris-HCl, pH 7.5) and then transferred to storage buffer (50 mM NaCl, 75 mM NaSCN, 20 mM Tris-HCl, pH 7.5) for a further 2 h. Protein concentration was measured using the Bio-Rad protein detection kit.

In Vitro Assays—Protein binding assays were conducted in a 20-μl reaction volume using 2 μl of STA buffer (25 mM Tris acetate, pH 8, 8 mM magnesium acetate, 10 mM KCl, 1 mM dithiothreitol, and 3.5% (w/v) polyethylene glycol 6000) with 5 μM PspF-(1–275) and increasing concentrations of PspA (5 ,10, and 20 μM). Samples were incubated for 10 min at 30 °C and analyzed by 4.5% non-denaturing polyacrylamide gel electrophoresis (25 mM Tris-HCl, pH 8, and 200 mM glycine at 4 °C). σ isomerization assays were conducted in 10-μl reaction volumes as described previously (12). Essentially, STA buffer containing 16 nM ^{32}P end-labeled heteroduplex DNA (mismatched at −12/−11, consisting of the −60 to 28 *Sinorhizobium meliloti nifH* promoter), 1 mM σ^{54}, 4 mM dGTP, and1 μM PspF-(1–275) was pre-incubated with either storage buffer or increasing concentration of PspA (0.5, 1, and 2.5 μM) in 4 μl of TGED (100 mM NaCl, 10 mM Tris-HCl, pH 8, 0.1 mM EDTA, 1 mM dithiothreitol, and 50% glycerol) for 10 min at 30 °C. This mixture was subsequently added to the σ isomerization assay for 10 min and analyzed using a 4.5% non-denaturing polyacrylamide gel in 25 mM Tris-HCl, pH 8, and 200 mM glycine at room temperature.

Size Exclusion Chromatography—Purified PspA (100 μl at 0.75 mg/ml) in SEC buffer (20 mM Tris pH 7.5, 50 mM NaCl, and 75 mM NaSCN) was analyzed on a Biosep SEC4000 column using a flow rate of 0.75 ml/min and a temperature of 4 °C. Fractions (0.75 ml) were collected between 2 and 15 min. Protein peaks were detected at 280 nm by a Beckman Coulter 166 Detector. The column was calibrated with the molecular mass standards of blue dextran (2000 kDa), thyroglobulin (669 kDa), ferritin (440 kDa), catalase (232 kDa), aldolase (158 kDa), bovine serum albumin (67 kDa), ovalbumin (43 kDa), and chymotrypsinogen (25 kDa), all at 2.2 mg/ml in SEC buffer.

Western Blotting—Proteins were separated by 15% SDS-PAGE (see Ref. 12) and electroblotted onto Immobilon-P membranes (Amersham Biosciences). Blots were blocked for 1 h in TBS (50 mM Tris-Cl, pH 7.5, and 150 mM NaCl) with 5% nonfat dried milk at room temperature and then incubated with α-PspA (*E. coli*), a kind gift from Louise Lloyd, Imperial College, at 1:10000 dilution in TBS with 5% nonfat dried milk. After washing in TBS plus 0.1% Tween 20, bound primary antibodies were labeled with horseradish peroxidase-conjugated rabbit anti-mouse (Sigma) at 1:8000 dilution in TBS and 5% nonfat dried milk. Secondary antibody binding was detected using the ECL chemiluminescence system (Amersham Biosciences) and Biomax XR film (Kodak).

Electron Microscopy and Image Processing—Samples were negatively stained using 2% (w/v) uranyl acetate prior to imaging on a Philips CM100 electron microscope at 80 kV and a magnification of 51,500×. Twenty micrographs for each sample, displaying no discernible drift or astigmatism, were digitized at a step size of 10 μm using a Leafscan 45 densitometer. The resultant sampling frequency of 1.94 Å/pixel on the specimen scale was coarsened by a factor of 2 to increase the speed of all subsequent processing using Imagic-5 software (17, 18). No correction was made for the contrast transfer function, given that the first minimum of the power spectrum for each micrograph was observed to be in the 18–21 Å range. A data set of 4,500 particles was built by interactively selecting all possible single particles observed. The data set was analyzed by reference-free alignment coupled with multivariate statistical analysis (19). A number of subpopulations within each data set were identified that displayed approximately top, side, or intermediate orientation. These numbered 1,100, 1,500, and 1,600 particles, respectively. Each of these subpopulations was treated *de novo* and iteratively refined to gain two-dimensional class averages with an improved signal-to-noise ratio (18). Reprojections were taken from the best three-dimensional model obtained and used to identify additional atypical views and further refine the subpopulation class averages. For three-dimensional reconstruction, class averages from each subpopulation were used that ensured the broadest range of relative orientations. Eulerian angles were assigned *a priori* by angular reconstitution (20) (see supplementary data in the on-line version of this article), and iterative refinements were implemented. The resolution of the final three-dimensional map, which was composed of ~50 class averages from each subpopulation data set, was estimated by Fourier shell correlation (17). Surface-rendered views, where presented, are shown with a threshold of 5σ, providing for 1,178,224 cubic Ångstroms. Assuming a standard density of 0.844 Da/Å^3, this equates to 1396 kDa. It should be noted, however, that proteins do differ in density, and the exact density of PspA remains unknown. Modeling studies were performed within the O software environment (21).

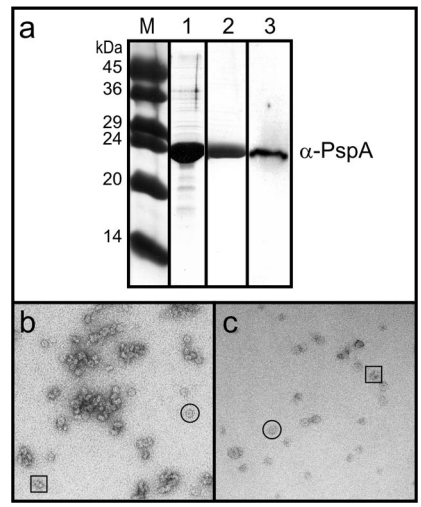

FIG. 1. **Purification of PspA complexes.** *a*, SDS-PAGE and Western blot analysis. *Lane M*, SDS-PAGE gel markers from Sigma (MW-SDS-70L at 14, 20, 24, 29, 36, 45, and 66 kDa); *lane 1*, SDS-PAGE lane of purified PspA (used for EM and prior to HPLC purification); *lane 2*, Western blot lane of purified PspA (used for EM and prior to HPLC purification); *lane 3*, Western blot lane of the 1,023 kDa peak of HPLC trace. *b*, electron micrograph of a typical PspA sample as used for image processing. *c*, electron micrograph of HPLC-purified 8.8 min peak sample. In *panels b* and *c* the assigned top views are *circled* and the side views are *boxed*.

RESULTS

Isolation and Purification of PspA Protein from E. coli—Crude CHAPS-solubilized extract containing His_6-tagged PspA was applied to a nickel affinity column (Fig. 1*a*, *lane 1*). Subsequent elution with imidazole (250 mM) yielded essentially pure His_6-tagged PspA as judged by SDS-PAGE (Fig. 1*a*, *lane 2*) and negative stain EM (Fig. 1*b*). In the latter, ring-like structures were evident. The activity of the PspA preparation was analyzed for its ability to form a complex with PspF-(1–275) and also inhibit σ isomerization. Indeed, it was able to do both (data not shown) (12). To ensure that the His_6 tags of the expressed PspA did not contribute to the organization of PspA

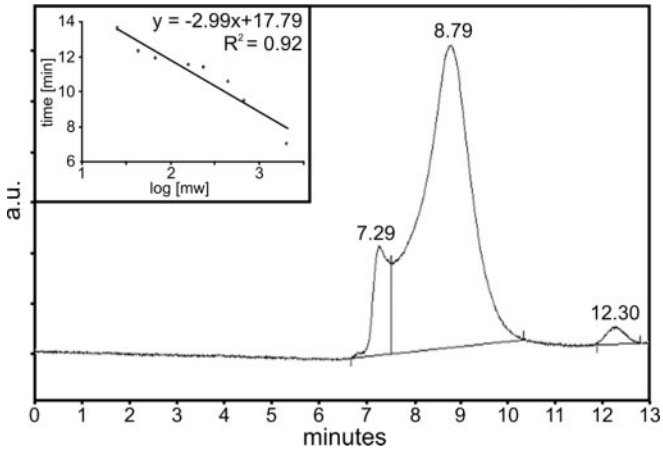

FIG. 2. **HPLC elution profile.** Peaks at 7.29, 8.79, and 12.30 min are highlighted, the former eluting in the void volume and the latter two corresponding to molecular masses of 1,023 and 69 kDa respectively. *Inset*, the standard curve (see "Methods and Materials").

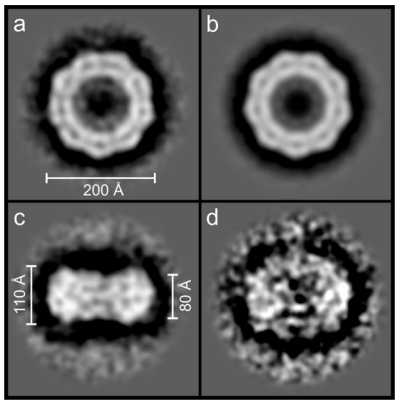

FIG. 3. **Single particle analysis of oligomeric PspA rings.** Shown are typical class averages observed from each of the three subpopulations, assigned as a top view of the PspA ring (unsymmetrized) (*a*), a top view of (C9 symmetrized) (*b*); an approximate side view (*c*), and a tilted view (*d*). The maximum dimensions were 200 Å diameter (top view) and thickness ranging between 110 (outer edge) and 80 Å, as indicated.

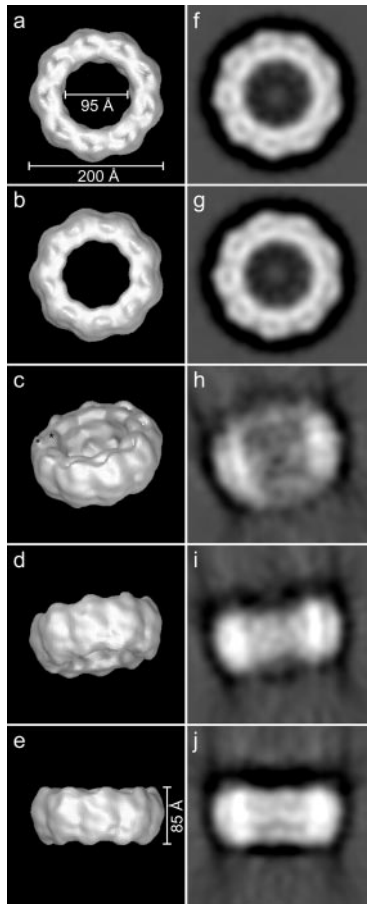

FIG. 4. **Characteristic views of the PspA oligomeric three-dimensional map at 30 Å.** *a–e*, surface-rendered views ranging from top to side, with *panel b* being the reverse of the top view in *panel a*. *f–j*, two-dimensional reprojections derived from the three-dimensional map at the same orientation to *panels a–e*. The three-dimensional map has dimensions of a 200-Å outer diameter, 95-Å inner diameter (top view), and a maximum thickness of 85 Å (side view) given the peak features present. The distance between the *starred* (*) peaks in *panel c* is 30 Å, indicating the presence of sub-domains.

oligomers into rings, the tags were enzymatically cleaved. Cleavage did not change the activity of PspA. No ring dissociation was observed,[2] confirming that the ring contacts were mediated by PspA and not the His_6 tag. To determine the molecular mass of the components of the PspA sample, the preparation was analyzed by size-exclusion HPLC (Fig. 2). Three main peaks with elution times of 7.29, 8.79 and 12.30 min were resolved. The first of these eluted in the void volume and consisted of the aggregated rings seen in Fig. 1*b*. The 8.79 and 12.30 min peaks correspond to apparent molecular masses of 1,023 kDa and 69 kDa, respectively. EM (Fig. 1*c*) and Western blot analysis (Fig. 1*a*; *lane 3*) of the 1023-kDa peak fraction confirmed that it consisted of PspA rings of similar structure. Given that the His_6-tagged PspA monomeric unit has a molecular mass of 27.9 kDa, this suggests a composition of 36–37 PspA subunits. The 12.30 min peak of 69 kDa indicates a composition of either PspA dimers (55.8 kDa) or trimers (83.7kDa)

Single Particle Image Analysis—The purified PspA complexes (see Fig. 3) were negatively stained, imaged and digitized to yield a 4,500-particle data set. Reference-free alignment and classification resolved particles into three populations, which were assigned to approximate top (1,100 particles), side (1,500 particles), and tilted (1,600 particles) views. The remainder of the single particle images (~300), which clearly contained more than one complex or stain artifact, were removed. Each subpopulation was treated *de novo*, and further iterative multi-reference alignments improved their signal-to-noise ratio. Representative two-dimensional average views for top, side, and tilted populations are shown in Fig. 3, *panels a*, *c*, and *d*, respectively. The top view in Fig. 3*a* is unsymmetrized but reveals a ring with nine distinct domains and an outer diameter of 200 Å. At the center of the ring, the black, stain-filled region (diameter 50 Å) is surrounded by features of weak contrast arranged in a ring with a diameter of 95 Å. The strongest features, attributable to protein density, lie between 95 and 200 Å diameter. The top view is presented in a 9-fold rotationally symmetrized (C9) form in Fig. 3*b* and has a resolution of 29.6 Å as calculated by Fourier ring correlation. Given that the calculated molecular mass from HPLC (1023 kDa) is within 2% of the theoretical mass of a 9 × 4 oligomer (1004 kDa), it seems likely that the PspA ring is composed of 36 PspA subunits. This result also suggests that the SEC-resolved 69 kDa peak is composed of PspA dimers rather than trimers, because in the latter case a 9 × 3 oligomeric PspA ring would have a much lower theoretical mass of 753 kDa than that observed.

[2] B. D. Hankamer, S. L. Elderkin, M. Buck, and J. Nield, unpublished data.

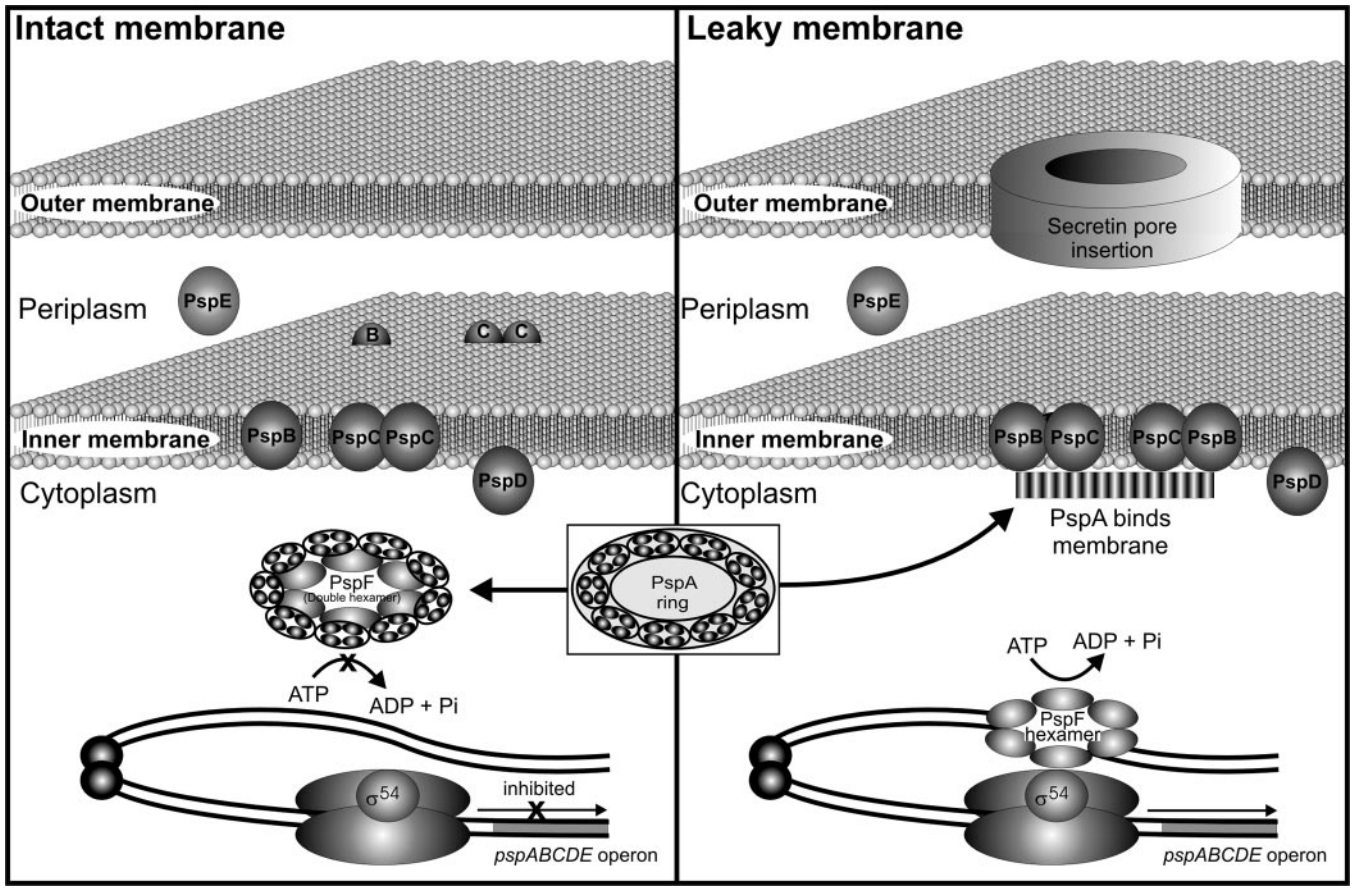

FIG. 5. **Functional model for PspA.** Each of the nine PspA ring domains resolved in this study is depicted containing four PspA subunits consistent with an apparent molecular mass of 1,023 kDa. Under "intact membrane" conditions, the PspA adapter protein inhibits the ATPase activity of PspF, possibly through the formation of a PspA ring·PspF complex. This inhibition of PspF blocks the transcription of the *pspABCDE* operon. Under "leaky membrane" conditions, PspC dimers located in the inner membrane are thought to dissociate into their monomeric constituents before interacting with PspB. PspA (either in the form of a ring or a smaller subcomplex) is then proposed to interact with PspB and PspC at the membrane surface, conferring protection during virulence factor export.

Fig. 3*c* is a characteristic "side" view that displays a width of 200 Å and a thickness ranging between 80 Å and 110 Å. Fig. 3*d* concludes with a characteristic "tilted" view.

Features of the Three-dimensional Map—Surface rendered views of the three-dimensional structure of the *E. coli* PspA ring complex, together with respective two-dimensional reprojections, are shown in Fig. 4. The three-dimensional map was low pass filtered to 30 Å, the overall resolution having been estimated to be in this range by Fourier shell correlation. The calculated map has a similar appearance to the two-dimensional averages and was verified as being C9 point group symmetric, *i.e.* containing nine sets of subunits. The protrusions observed on either surface are different, and, at this resolution, each domain appears to contain four subdomains, such as those features within each domain separated by a distance of 30 Å, which are shown starred (*) in Fig. 4*c*. Overall, the final three-dimensional map has maximum dimensions of 200 Å in diameter with a maximum measured thickness of 85 Å. The three-dimensional map is effectively an average of all its constituent two-dimensional characteristic views, and the reprojection side view shown (Fig. 4*e*) has crenulated horizontal edges that vary the overall thickness. It is also important to note that possible effects due to the use of negative stain, *e.g.* dehydration, may occur and that a relative lack of direct two-dimensional side views was observed. Bearing these in mind, we suggest that the thickness of the three-dimensional map should be considered to be in a range of 80 to 110 Å.

DISCUSSION

We have calculated the first structural data for PspA. PspA was found to form a 9-fold symmetric ring having a HPLC-derived molecular mass of 1023 kDa. PspA is an important *E. coli* protein that plays a role in both the regulation of the *psp* operon through inhibition of the transcription activator AAA⁺ protein PspF and in the maintenance of the proton motive force and membrane integrity. Interactions with other Psp proteins are thought to be important for PspA functioning (5, 12, 22). PspA has recently been classified as an adaptor protein having modulation effects on the AAA⁺ protein PspF. Members of the adaptor protein family share no sequence homology, are structurally unrelated, but are generally small, with a common function in that they modulate the activity of AAA⁺ proteins. In this regard, it is of interest that we have found PspA to form a large macromolecular complex. The full biological significance of such a ring structure is unknown. Dimensions of a 200-Å diameter with ~85-Å thickness in our final three-dimensional map may be compared with that of a typical AAA⁺ protein complex, the PspF hexamer ring, which has been suggested by cryo-EM to be dimeric with a diameter of ~140 Å and thickness of 110 Å (23). These dimensions are thought to be characteristic of other AAA⁺ proteins, such as those found by cryo-EM and modeling studies of p97 (24–26).

An oligomer assembly and/or disassembly may act as an on/off switch for PspA functions, one of which is inhibition of PspF (Fig. 5). We have shown that our PspA samples, which

consisted predominantly of C9 symmetric rings, completely inhibit PspF-(1–275) activity at a ratio of 1 PspF/2.5 PspA subunits (12). The PspF-(1–275)·ADP·AlF_x complex is likely to be a dimer of hexamers (23), indicating that a 12:36 PspF·PspA complex might form. Such a complex seems likely to be associated with inhibition, although we do not know whether initial complexes between PspA and PspF oligomers lead to further complexes in which important changes in subunit structure have occurred. The above dimensions of PspF and PspA suggest that complex function is possible through the interaction of the PspA ring and a PspF double hexamer. PspA has a membrane-related function reported to be mediated through protein-protein interactions involving the Psp proteins PspB and PspC (10, 22). These proteins are integral membrane proteins, and the periplasmic domains of PspC are able to form a dimer under normal conditions (22). Alterations in the stability of the membrane and dissipation of the proton motive force may induce disassociation of the PspC dimer, which is then able to interact with PspB and form a complex that preferentially binds to PspA, either in the dimeric or ring-like form (Fig. 5) (22, 23). This would provide a method of regulation in that, under different cellular concentrations or conditions, PspA is more or less able to interact with PspB and PspC as opposed to PspF. The pIV secretin has been visualized by electron cryomicroscopy at a resolution of 22 Å, displaying dimensions of a 135-Å diameter and a length of 240 Å with a central pore diameter of 60–88 Å, and, being a D14 symmetric barrel-like structure, a dimer of two 14-multimer rings (27). How this secretin is able to induce induction of the *psp* response remains unknown.

In one membrane-bound form, PspA may release PspF from its inhibited state, thereby allowing the transcription of the *psp* operon, the products of which have been reported to facilitate the stability of the membrane and proton motive force (10, 22). When membrane stability is no longer compromised, PspC may be free to dimerize, releasing PspB and PspA. Subsequently, PspA may again bind PspF, thereby acting in its inhibitory role and thus preventing further transcription of the *psp* operon. Evidence to support such a PspC monomer/dimer proposal originates from the Tim23 protein found in mitochondria, which is involved in the protein import machinery. It has a leucine zipper motif and forms a dimer in response to changes in membrane potential (22). The nonameric ring-like structure of PspA opens up the possibility of interaction with the F_1 membrane-bound ATPase, where symmetry match and mismatch would become significant.

In terms of subunit structure, it is also of note that PspA has a high sequence homology with the VIPP1 protein found in photosynthetic membranes. VIPP1 forms a coiled-coil structure, with a large coiled-coil region spanning residues 1–186 and a second smaller coiled-coil region spanning residues 187–222. VIPP1 plays an essential role in thylakoid biogenesis and has no known transcriptional regulatory functions or any role in modulating AAA$^+$ proteins (15, 16). Although this indicates that VIPP1 is not a member of the adaptor protein family, its structure could potentially shed light on the membrane-bound form of PspA and the role it plays in the bacterial protein export process.

Acknowledgments—We acknowledge Drs. Susan Jones, Pampa Ray, Bernadette Byrne, and Fabienne Beuron for additional support.

REFERENCES

1. Koster, M., Bitter, W., and Tommassen, J. (2000) *Int. J. Med. Microbiol.* **290,** 325–331
2. Hardie, K. R., Lory, S., and Pugsley, A. P. (1996) *EMBO J.* **15,** 978–988
3. Darwin, A. J., and Miller, V. L. (2001) *Mol. Microbiol.* **39,** 429–444
4. Kleerebezem, M., and Tommassen, J. (1993) *Mol. Microbiol.* **7,** 947–956
5. Kleerebezem, M., Crielaard, W., and Tommassen, J. (1996) *EMBO J.* **15,** 162–171
6. van Der Laan, M., Urbanus, M. L., Ten Hagen-Jongman, C. M., Nouwen, N., Oudega, B., Harms, N., Driessen, A. J., and Luirink, J. (2003) *Proc. Natl. Acad. Sci. U. S. A.* **100,** 5801–5806
7. Jones, S. E., Lloyd, L. J., Tan, K. K., and Buck, M. (2003) *J. Bacteriol.* **185,** 6707–6711
8. Eriksson, S., Lucchini, S., Thompson, A., Rhen, M., and Hinton, J. C. D. (2003) *Mol. Microbiol.* **47,** 103–118
9. Darwin, A. J., and Miller, V. L. (1999) *Mol. Microbiol.* **32,** 51–62
10. Model, P., Jovanovic, G., and Dworkin, J. (1997) *Mol. Microbiol.* **24,** 255–261
11. Jovanovic, G., Rakonjac, J., and Model, P. (1999) *J. Mol. Biol.* **285,** 469–483
12. Elderkin, S., Jones, S., Schumacher, J., Studholme, D., and Buck, M. (2002) *J. Mol. Biol.* **320,** 23–37
13. Dworkin, J., Jovanovic, G., and Model, P. (2000) *J. Bacteriol.* **182,** 311–319
14. Dougan, D. A., Mogk, A., Zeth, K., Turgay, K., and Bukau, B. (2002) *FEBS Lett.* **529,** 6–10
15. Westphal, S., Heins, L., Soll, J., and Vothknecht, U. C. (2001) *Proc. Natl. Acad. Sci. U. S. A.* **98,** 4243–4248
16. Kroll, D., Meierhoff, K., Bechtold, N., Kinoshita, M., Westphal, S., Vothknecht, U. C., Soll, J., and Westhoff, P. (2001) *Proc. Natl. Acad. Sci. U. S. A.* **98,** 4238–4242
17. Van Heel, M., Gowen, B., Matadeen, R., Orlova, E. V., Finn, R., Pape, T., Cohen, D., Stark, H., Schmidt, R., Schatz, M., and Patwardhan, A. (2000) *Q. Rev. Biophys.* **33,** 307–369
18. Ruprecht, J., and Nield, J. (2001) *Prog. Biophys. Mol. Biol.* **75,** 121–164
19. Van Heel, M., Harauz, G., Orlova, E. V., Schmidt, R., and Schatz, M. (1996) *J. Struct. Biol.* **116,** 17–24
20. Van Heel, M. (1987) *Ultramicroscopy* **21,** 111–123
21. Jones, T. A., and Kieldgaard, M. (1993) *O Version 5.9, The Manual*, Uppsala University, Uppsala, Sweden
22. Adams, H., Teertstra, W., Demmers, J., Boesten, R., and Tommassen, J. (2003) *J. Bacteriol.* **185,** 1174–1180
23. Zhang, X., Chaney, M., Wigneshweraraj, S. R., Schumacher, J., Bordes, P., Cannon, W., and Buck, M. (2002) *Mol. Microbiol.* **45,** 895–903
24. Zhang, X., Shaw, A., Bates, P. A., Newman, R. H., Gowen, B., Orlova, E., Gorman, M. A., Kondo, H., Dokurno, P., Lally, J., Leonard, G., Meyer, H., van Heel, M., and Freemont, P. S. (2000) *Mol. Cell* **6,** 1473–1484
25. Beuron, F., Flynn, T. C., Ma, J., Kondo, H., Zhang, X., and Freemont, P. S. (2003) *J. Mol. Biol.* **327,** 619–629
26. Bordes, P., Wigneshweraraj, S. R., Schumacher, J., Zhang, X., Chaney, M., and Buck, M. (2003) *Proc. Natl. Acad. Sci. U. S. A.* **100,** 2278–2283
27. Opalka, N., Beckmann, R., Boisset, N., Simon, M. N., Russel, M., and Darst, S. A. (2003) *J. Mol. Biol.* **325,** 461–470

Euler angle map Supplementary material

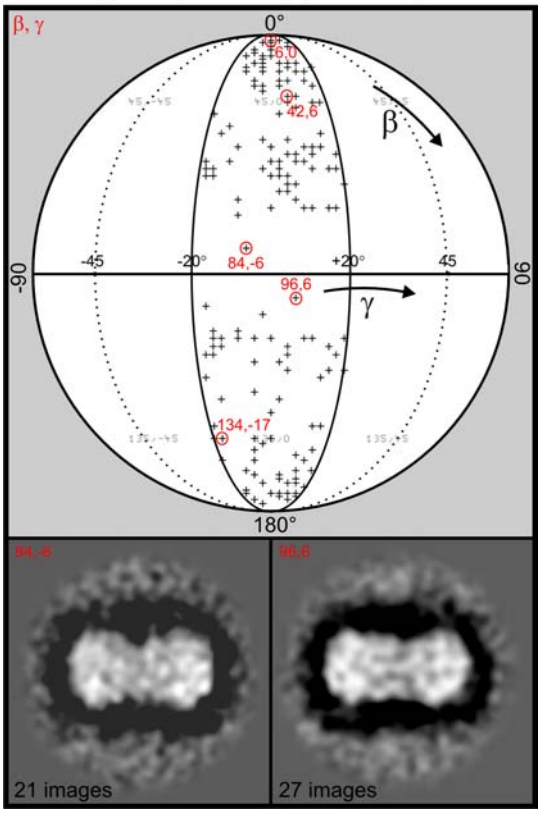

Organization of the AAA$^+$ Adaptor Protein PspA Is an Oligomeric Ring

Ben D. Hankamer, Sarah L. Elderkin, Martin Buck and Jon Nield

J. Biol. Chem. 2004, 279:8862-8866.
doi: 10.1074/jbc.M307889200 originally published online December 19, 2003